On the Risk of Hydraulic Fracturing in CO2 Geological Storage

Panos Papanastasiou
Department of Civil and Environmental Engineering, University of Cyprus, 1678 Nicosia, Cyprus

Euripides Papamichos
Department of Civil Engineering, Aristotle University of Thessaloniki, GR-54124 Thessaloniki, Greece

Colin Atkinson
Department of Mathematics, Imperial College London, SW7 2AZ, London, United Kingdom

SUMMARY

We present a contribution on the risk of hydraulic fracturing in CO2 geological storage using an analytical model of hydraulic fracturing in weak formations. The work is based on a Mohr-Coulomb dislocation model that is extended to account for material with fracture toughness. The complete slip process that is distributed around the crack tip is replaced by superdislocations that are placed in the effective centers. The analytical model enables the identification of a dominant parameter which defines the regimes of brittle to ductile propagation and the limit at which a mode-1 fracture requires infinite energy to advance. We examined also how the corrosive effect of CO2 on rock strength may affect the hydraulic fracture propagation. We found that a hydraulically induced vertical fracture from CO2 injection is more likely to propagate horizontally than vertically, remaining contained in the storage zone. The horizontal fracture propagation will have a positive effect on the injectivity and storage capacity of the formation. The containment in the vertical direction will mitigate the risk of fracturing and migration of CO2 to upper layers and back to the atmosphere. Though the corrosive effect of CO2 is expected to decrease the rock toughness and the resistance to fracturing, the overall decrease of rock strength promotes the ductile behavior with the energy to dissipate in plastic deformation and hence mitigates the mode-1 fracture propagation.

Key words: carbon geological storage, CO2 sequestration, caprock, risk of fracturing, hydraulic fracturing, plasticity, Mohr-Coulomb dislocation.

1. INTRODUCTION

According to the latest International Energy Association reports the CO_2 capture and storage (CCS) must be part of the strategy for mitigating climate changes and keep the increase in the global temperature below the 2^oC threshold. Towards achieving this target by 2040 the international community must invest every year near 1.6 trillion dollars with the biggest share spending, in Efficiency, Renewables, Nuclear and Carbon Capture and Storage (CCS). The recommended capital investment in CCS projects is of the order of 75 billion/year and is expected to contribute 13% to the global cumulative CO2 reductions by 2050 [1]. Though related technologies for CCS projects has been extensively developed in the Oil and Gas industry it still remains expensive to be materialized. For the time being CCS projects are economically viable when they are combined with other technologies such as enhanced oil recovery. Nevertheless, deployment of CCS project at large scales in the near future is a matter of policy decision of the international community on the climate change issue [2, 3].One of the outstanding issues of the CO2 geological storage which must be addressed by the research community is the risk of CO2 leakage with potential contamination of shallow water and soil resources or escape back to the atmosphere. In depleted oil and gas fields, the existence of a sealing capacity to hydrocarbons and eventually to CO2, is demonstrated by the very existence of the field. Such demonstration does not exist for the case of saline aquifers, although analogies are likely to be found. In addition, a cap rock that might be adequate for oil and gas storage may not be adequate for CO2 storage due to its corrosive action or to the different operating pressures. Therefore, determination of cap rock sealing properties by testing and modelling is required [4]. There are many mechanisms of CO2 migration to the upper layers and to the atmosphere. In geological basins that were exploited for hydrocarbon exploration and production, mainly in USA, there are 1000s of abandoned unshielded wells, with no-existence or bad casing and cement which could serve as conduit of CO2 leakage to upper layers or to the atmosphere. CO2 can also move upwards through diffusion or if the CO2 column pressure exceeds the capillary pressures of the saline water in the cap rock. CO2 can migrate upwards through non-sealing faults or through induced hydraulic fracturing if the CO2 pressure exceeds the closure stress defined by the minimum insitu stress. There are many related issues in CCS operations such as, to mention few, the well injectivity, the brine displacement by the CO2, the build-up of the pressure under the

caprock [5,6,7], the storage capacity [8] and the hydro-chemo-mechanical behavior and rock dissolution from the corrosive action of the CO2 injection [9, 10,11].

In this study we will investigate the risk of CO2 escape through induced mode-1 fracturing of the formation. We extended an earlier work on the modeling of hydraulic fracturing in weak formations to study in particular the risk of induced vertical hydraulic fracture that it will propagate in the vertical vs horizontal direction. Propagation of hydraulic fracturing in the vertical direction is unwanted as imposes risk of upward migration while propagation in the horizontal direction could be beneficial as it will increase the CO_2 injectivity and storage capacity of the formation. Furthermore, we studied the same risk by modifying some mechanical parameters of the rock because it is expected that CO_2 injection under supercritical conditions will change the properties of the reservoir and cap rock due to its corrosive action. We clarify here that the down-hole temperature and pressure conditions at which the CO2 is injected in the formation are higher than the critical temperature (31.1 °C) and critical pressure (7.38 MPa) above which the CO2 adopt properties midway between a gas and a liquid. It behaves as a supercritical incompressible fluid with high density, which has gas flow behavior and strong dissolution ability. Though there is no clear evidence that frictional equilibrium and instabilities are affected by CO2 storage [12] we assumed in this study some extreme degradation of fracture toughness and cohesion to consider a worst case scenario.

This work is based on an analytical model of hydraulic fracturing in weak formations which accounts for plastic yielding that may develop near a hydraulic fracture tip. The model is built on dislocation theory for Mohr-Coulomb pressure sensitive material that accounts for small [13] and large scale yielding that surrounds the crack tip [14]. Small scale yielding corresponds to the case where the irreversible deformation is contained in a small region near the tip which its size is much smaller than the fracture length whereas in the large scale yielding the size of the plastic zone becomes important relative to the fracture length. Plastic yielding describes the irreversible deformation in the form of distributed normal and shear dislocations. In order to derive analytical solutions, the effect of distributed dislocations or plasticity is replaced here by super-dislocations that are placed in the effective centers of the complete slip process that is distributed around the crack tip. In this work we extended the dislocation model to account for finite rock fracture toughness which was neglected in the earlier studies. The analytical model enables the identification of a dominant parameter that defines the regimes of brittle to ductile

fracture propagation and the limit beyond which no fracture can propagate in mode-1 as it will require infinite energy.

The article is structured as follows: In the next section, we describe the motivation behind this work. In Section 3 we present the extension of the Mohr-Coulomb dislocation hydraulic fracturing model to account for finite fracture toughness and for large scale yielding. Results are presented and discussed in Section 4 for frictionless and frictional materials as function of a dominant parameter that defines the brittle to ductile regimes. The main conclusions are drawn in Section 5.

2. FROM BRITTLENESS TO DUCTILITY IN HYDRAULIC FRACTURING

The present work was motivated by the findings of earlier studies on the problem of hydraulic fracturing in weak rocks. Those studies were carried out in order to explain the high net-pressures observed in hydraulic fracturing operations in the field and the discrepancies between simulators and field measurements, which was an issue that was highly debatable in the early nineties. Relevant to the topic of this paper are the numerical studies in references [15,16,17,18] which investigated the influence of plastic deformation in hydraulic fracturing using a coupled elastoplastic hydraulic fracturing model based on finite element analysis. Relevant experimental work can be found in [19]. It has been shown that plastic yielding near the tip of a propagating fracture provides an effective shielding, resulting in a significant increase of the rock effective fracture toughness [17]. A fracture that propagates in a weak plastically deformed formation (plastic fracture) is shorter and wider than the fracture that propagates in a strong elastic formation (elastic fracture) of the same volume and hence a higher pressure is needed to propagate a plastic fracture than an elastic fracture [16, 17, 18].

We recall in particular from [17] results that show the influence of plastic yielding on the apparent or effective fracture toughness increase in hydraulic fracturing (Table 1). In those studies the fractures were propagated using cohesive interface elements for propagation criterion and the unknown values of effective fracture toughness were determined during propagation using the J-integral [20] and were recorded once the plastic zones were fully developed. Interaction at the pore-scale between crystal plasticity and fracturing which can explain the mechanism of fracture toughness was studied in [21].

Rock strength [MPa] / Insitu stresses [MPa]	σ_C=60 σ_T=6	σ_C=20 σ_T=6	σ_C=20 σ_T=2
σ_1=30, σ_3=30 $\frac{\sigma_1}{\sigma_3} = 1$	2.0	2.0	2.0
σ_1=45, σ_3=30 $\frac{\sigma_1}{\sigma_3} = 1.5$	2.0	4.60	7.31
σ_1=60, σ_3=30 $\frac{\sigma_1}{\sigma_3} = 2$	2.0	7.03	15.48

Table 1. Apparent fracture toughness [MPa m $^{1/2}$] determined from J-integral for a hydraulic fracture propagation based on cohesive elements for different values of in-situ stresses and rock strength [9].

The varying parameters in the table are the uniaxial compressive strength, σ_C, and the uniaxial tensile strength, σ_T, and the values of the insitu stresses. The main conclusion from Table 1 relevant to this paper is that for the same rock parameters the brittleness or ductility, expressed here by the calculated apparent fracture toughness, is a strong function of the stress field anisotropy. Plastic yielding does not take place under a hydrostatic field, even in weak formations (σ_c/σ_T= 20/2) and the effective fracture toughness remains equal with the input parameter in the constitutive definition of the interface elements, $K_{IC} = 2\ MPa\sqrt{m}$. For strong rock formation (σ_c/σ_T= 60/6), plastic yielding does not take place even in a highly non-hydrostatic stress-field. In other words, the brittleness or ductility in hydraulic fracturing is a function of both rock strength and stress field and cannot be considered in isolation as a function of one parameter. As we will see next, the stress-field relevant to fracture plane depends on the direction that the fracture front will propagate.

3. DISLOCATION MODEL FOR FRACTURING

We start with a planar vertical fracture which can propagate in any direction in the vertical fracture plane. For the deformation near the fracture front one may assume, within a good approximation, that plane strain conditions prevail, assumption which becomes fully valid for a front with infinite curvature. Furthermore, the plane strain condition is maintained if the height of the fracture is relatively large compared to the fracture length. We will consider here the two extreme cases of a plane strain fracture that propagates horizontally or vertically. In both cases the fracture plane has the same orientation, perpendicular to the direction of the minimum insitu stress, $\sigma_3=S_{hmin}$, which it is assumed to be horizontal and hence the fracture plane is vertical. In the case of the horizontal propagation, the fracture front will move along the direction of the intermediate insitu stress which can be assumed here to have a value close to the minimum insitu stress, $\sigma_1=S_{Hmax}$. In the case of vertical propagation, the fracture front will move upwards along the direction of the vertical insitu stress which can be assumed here to be the maximum stress $\sigma_1=S_v$, as in most cases of sedimentary basins. We emphasize here that a plane strain hydraulic fracturing model for a vertical fracture modeled by elasticity cannot differentiate between propagation direction (horizontally or vertically) as the only insitu stress that enters in the model is the stress perpendicular to the fracture plane which is minimum insitu stress. This stress, which is called confining or closure stress, defines the orientation of the fracture plane and the so called net-pressure which is the difference of the fracture internal pressure minus the closure stress. In the present model we take into account values of the stress along the propagation direction which can vary from a value equal to the minimum insitu stress (horizontal propagation) to a maximum value equal to the vertical insitu stress (vertical propagation).

Along these lines, we consider a pressurized plane strain fracture of length 2α which is embedded in a non-isotropic stress field with the minimum compressive stress σ_3 acting in the direction, y, normal to the fracture plane and the maximum compressive stress, σ_1, acting parallel to the crack plane along the propagation direction x (Fig.1). Pressurization of a fracture produces a non-uniform stress relief from the original compressive in situ stress field resulting in a high shear stress concentration around the fracture tip. In weak rocks, such as poorly consolidated sandstones or soft shales, large inelastic deformation is expected to take place in the area near the crack tip due to the excessive shear stress concentration. The stress relief, the high shear stress and the plastic deformation is driven by the decrease of the minimum stress and the

consistency condition which requires the state of stress to remain on the yield or loading surface during plastic flow. The plastic rock deformation in this study is described by the Mohr-Coulomb model which takes into account the pressure-sensitive frictional behavior of rocks.

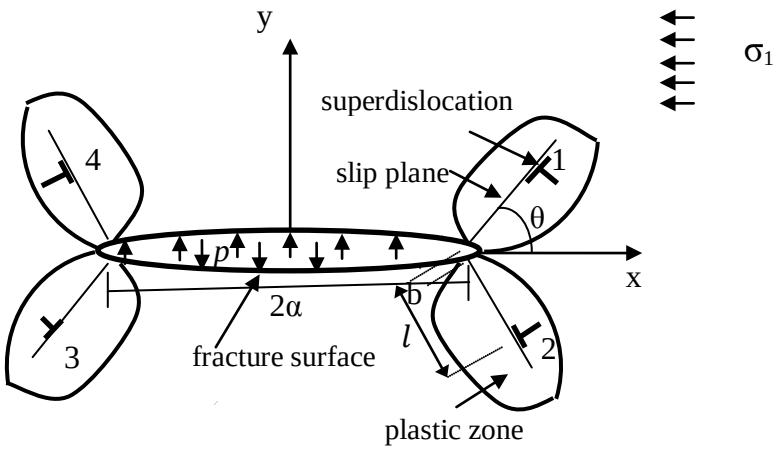

Fig.1. Schematic representation of the dislocation model

The injection of the CO2 in supercritical conditions in the formation is constrained by the displaced saline water or any other resident fluid and the low permeability of the cap rock. The continuing injection operation may increase the CO2 fluid pressure to a value that may initiate a short crack from a pre-existing defect and turn it into a propagating hydraulic fracture. Under these operations it is reasonable to assume that the fluid pressure, *p*, of the CO2 acting on the short fracture is constant along the fracture length. In other words, we neglect any viscous pressure drop along the fracture. More general loadings can be considered without much difficulty but it is out of the scope of this study. Furthermore, the constant pressure is a reasonable assumption for a plastic fracture, compared to an elastic fracture, because the former is shorter and wider resulting in a uniform pressure along the fracture with almost all the pressure drop taking place very near to the fracture tip [15,16,17,18,19]

The net-pressure which as a dominant parameter in hydraulic fracturing is defined by (compressive stresses are positive)

$$\sigma = p - \sigma_3 \tag{1}$$

and is connected with the stress intensity factor for an elastic material via

$$K_{el} = \sigma\sqrt{\pi\alpha} \tag{2}$$

Therefore, loading of the fracture can be expressed through the net-pressure, σ, or through the stress intensity factor (SIF), K_{el} .

Plastic yielding, whose extent depends on material strength and loading conditions, is expected to take place around the fracture tip due to the high shear stress concentration (Fig. 1). For small scale yielding the plastic zones have the so-called 'rabbit ears' shape. In the dislocation model [13,14] each distributed plastic zone is replaced by a superdislocation pair placed at the effective centre of plastic yielding, which is defined by $z = \alpha + le^{i\theta}$, where θ is the angle between the crack plane and slip plane and l is the distance from the crack tip along the slip plane (Fig.1).

The unknown positions and strengths of the super-dislocations will be determined next from the following three conditions:

(i) the total stress-intensity factor at the crack tip is equal to the material fracture toughness K_{IC}. This can be related to the local energy release rate at the crack tip. In the earlier studies the fracture toughness K_{IC} was set to zero but in this study it will not be ignored but it will be further degraded due to the CO2 corrosion effect.

(ii) a local frictional equilibrium condition at the superdislocation position requires the total stresses minus the self stresses of the superdislocation to satisfy the Mohr-Coulomb yield criterion

(iii) the total crack opening displacement (COD) produced by the dislocation model is maximized; this condition assumes that the crack will so act to maximize its opening.

The first condition (i) satisfies the propagation criterion at the crack-tip and it is expressed by

$$\sigma\sqrt{\pi\alpha} - \frac{1}{8(\pi\alpha)^{1/2}}\frac{E}{(1-\nu^2)}b\,f = K_{IC} \tag{3}$$

where the first term is due to the external loading (net-pressure) whereas the second term gives the contribution of the dislocation internal stress field -crack interaction to the stress intensity factor. E and ν are the elastic modulus and Poisson's ratio, respectively, and b denotes the dislocation strength. The function f is given as [22]

$$f = \frac{8\ \sin\theta}{D}\left[\cos\frac{\theta+\beta}{2} + \frac{\frac{l}{\alpha}}{D^2}\cos\frac{\theta+3\beta}{2} + \frac{(l/\alpha)^2}{D^2}\cos\frac{\theta-3\beta}{2}\right] \quad (4)$$

where

$$\beta = \cos^{-1}\frac{2\left(\frac{l}{\alpha}\right)+\left(\frac{l}{\alpha}\right)^2\cos\theta}{D^2} \qquad \text{and} \qquad D = \frac{l}{\alpha}\left\{1 - 4\left(\frac{l}{\alpha}\right)^2\left[1 + \frac{l}{\alpha}\cos\theta\right]\right\}^{1/4}$$

The dislocation strength b is derived from the combination of equations (2), (3) and (4) as

$$b = (K_{el} - K_{IC})\ 8\sqrt{\pi\alpha}\ \frac{(1-\nu^2)}{E}\frac{1}{f} \quad (5)$$

From the second condition (ii), force equilibrium at the dislocation centre is specified in terms of the shear stress, τ and the normal stress, σ_n,which must satisfy the Mohr-Coulomb yield criterion

$$\tau + \sigma_n \tan\varphi = c \quad (6)$$

where, φ and c are the material friction angle and cohesion, respectively. If for some combination of the insitu stresses and the inclination of the superdislocation positions, the normal stress, σ_n, is tensile the 2nd term in (6) is neglected. The same treatment is applied for the case of frictionless or undrained condition. In both cases the dislocation model degenerates back to the original von Mises dislocation model which was originally developed for metals.

The shear stress at the dislocation center is given by

$$\tau = \sigma h + \frac{G}{4\pi(1-\nu)}b(g+k) + \frac{(\sigma_1-\sigma_3)}{2}\sin(2\theta) \quad (7)$$

where the first term is due to the crack loading, the second term gives the contribution of the opposite dislocation placed at position $z = \alpha + le^{-i\theta}$, and the last term is due to the original in situ stress field. The functions appearing in (7) are derived in [22] as

$$h = \sin\theta\left[\cos\theta + \frac{l/\alpha}{D^3}\cos\frac{\theta-3\beta}{2}\right] \quad (8)$$

$$g = \frac{2(\frac{l}{\alpha})\sin^2\theta}{D^2}\left[-\frac{3}{2D^2}\cos 2\beta - \frac{2(\frac{l}{\alpha})\cos(\theta-2\beta)}{D^2} - \left(\frac{l/\alpha}{D}\right)^2\cos(2\theta-2\beta) - \frac{\sin(2\beta)}{2\,l/\alpha\sin\theta}\right.$$

$$\left. + \frac{\sin(\theta-2\beta)}{2\sin\theta} - \frac{(\frac{l}{\alpha})\cos(3\beta)}{D^4} - \left(\frac{l/\alpha}{D^2}\right)^2\cos(\theta-3\beta) - \frac{\sin(\beta)}{2\,D^2\sin\theta} - \frac{D^2}{2(l/\alpha)^2}\right] \quad (9)$$

$$k = -\frac{\cos 2\theta}{\alpha(l/\alpha)} \quad (10)$$

The normal stress σ_n at the dislocation is derived similarly as

$$\sigma_n = \frac{K_{el}}{(2\pi l)^{1/2}}\left[\frac{\cos\theta/\sin\theta+\sin(2\theta)-(3/2)\sin\theta\cos\theta/2^2}{6\sin\theta\cos(\frac{\theta}{2})}\right]+\frac{(K_{el}-K_{IC})}{(2\pi l)^{1/2}}\cos\left(\frac{\theta}{2}\right)^3 - \frac{K_{el}}{(\pi\alpha)^{1/2}} - \frac{(\sigma_1+\sigma_3)}{2} +$$

$$\frac{(\sigma_1-\sigma_3)}{2}\cos(2\theta) \quad (11)$$

The first and second term in (11) were derived under the assumption of the small scale yielding. However, we expect that the biggest contribution to the normal stress σ_n arises from the last two terms which express the contribution of the initial stress field (σ_1, σ_3).

Next, we substitute the expressions (7) and (11) for the shear stress τ and normal stress, σn, in the Mohr-Coulomb criterion (6) which can be resolved for the dislocation position, l/α. As mentioned earlier, a tensile normal stress σ_n, it is not taken into account in the Mohr-Coulomb criterion since it does not provide any frictional resistance to sliding.

Once l is determined the dislocation strength b is calculated from (5). The crack-opening displacement due to the dislocation slip is given by

$$\delta = 2\,b\sin\theta \quad (12)$$

The above equations still include as an unknown the angle θ of the slip band on which the superdislocation lies. It is determined in the present model, according to condition (iii) to be the angle which maximizes the crack opening displacement (Fig. 1).

A related parameter of interest in this study is the force on the dislocations. Using the definition of force on a dislocation we get the quantity

$$F = 2\,b\,\tau \quad (13)$$

for the force produced on the two superdislocations emitted from one crack tip. τ is the finite shear stress (i.e. the total stress minus the self stress of the dislocation). Thus if we assume that the whole picture during crack propagation is self-similar F is the energy released per unit advance at the dislocations.

A particularly interesting case was the small scale yielding where the above equations were simplified allowing the determination of the important parameters. Small scale yielding was studied in reference [13] assuming, $l \ll \alpha$ and large scale yielding in [14] for the case of zero material fracture toughness, $K_{IC} = 0$. In the case of the small scale yielding and zero fracture toughness, the functions f, h, g, k are simplified allowing a closed form solution for the dislocation length l. A careful consideration of equations reveals that both the insitu stresses and the rock strength can be combined to the following dominant single parameter

$$t = \frac{(\sigma_1 - \sigma_3)}{2c\cos\varphi + (\sigma_1 + \sigma_3)\sin\varphi} \tag{14}$$

which will be used to present the results of the following section in a compact form. This parameter is also proposed as the brittleness index in hydraulic fracturing [23], in addition to other definitions which were based on material properties [24, 25].

4. RESULTS

4.1 Model parameters

A series of parametric studies has been carried out for particular cases to show that the Mohr-Coulomb dislocation model can capture the essential dependence of the crack-tip plasticity on the important parameter of Eq.(14) and to compare the propagation of a vertical fracture in horizontal and vertical directions. As it is mentioned in the introduction, propagation in the vertical direction is an unwanted phenomenon as the risk of CO2 escape will increase whereas propagation in the horizontal direction will have positive effects on the injectivity and storage capacity of the formation. Furthermore, we will make similar comparisons for the case of a formation with the original material properties vs the case with material properties degraded by the CO2 corrosive action to an extreme degree. We will present results for both small scale yielding and large scale yielding.

Table 2 presents the material parameters that were used in the computations. It was assumed that the material is isotropic. The value of the minimum insitu stress, which is in the

direction perpendicular to the fracture plane, is kept constant where as the stress, which is acting parallel to the direction of the propagation, varies from the value of the minimum stress to the value for which the model predicts that no mode-1 fracture will propagate. In additional computations, we assumed that the CO2 injection due its corrosive action will damage the material parameters to the extreme values shown in Table 2. It was assumed that the elastic material parameters and the friction angle will remain unchanged where as the material cohesion and fracture toughness will degrade by 10 times. Recent experimental results have shown that the degree of degradation is much less [26]. Nevertheless, we used here extreme values to bound any corrosive effects. It is reasonable to assume that the alteration of the fracture toughness is proportional to the alteration of the tensile strength which may be also proportional to the material cohesion.

	Original material	*Damaged material*
Elastic constants Elastic modulus Poisson's ratio	 E=10 GPa ν=0.3	
Plastic constants Friction angle Cohesion Undrained cohesion	 $\varphi = 30^0$ c = 10 MPa c_u = 10 MPa	 $\varphi = 30^0$ c=1 MPa c_u =1 MPa
Fracturing parameters Fracture toughness	K_{IC} = 1 MPa $m^{1/2}$	K_{IC} =0.1 MPa $m^{1/2}$
In-situ effective stresses Minimum insitu stress (horizontal) Maximum insitu stress (vertical)	 σ_3=25 MPa σ_1=25 to 100 MPa	
Fracture loading Stress Intensity Factor	SIF = 2 MPa $m^{1/2}$	

Table 2. Input Parameters

In the next figures we plotted the results of the calculated quantities which were derived for the small scale yielding assumption and the results of large scale yielding vs the dominant parameter of eq. (14). The calculated quantities are the dislocation length, l, the strength of the

dislocation, b, the crack opening displacement, δ and the dislocation force, F , for varying loading conditions and material parameters expressed through the single parameter of Eq.(14) . These values were calculated for the value of angle θ that maximizes the crack opening displacement, δ. The corresponding critical value of θ is also shown in these graphs.

4.2 Frictionless material

Figure 2 and 3 shows the results for a frictionless material or undrained analysis, which will be valid in the case of rapid fracturing in low permeability reservoir or caprock such as the shale formations, for small scale yielding and large scale yielding, respectively. The calculated quantities were plotted as a function of the loading parameter, derived from (14), for $\varphi = 0^0$

$$t = \frac{(\sigma_1 - \sigma_3)}{2c_u} \tag{15}$$

where c_u is the undrained cohesion of the material.

We observe that all the quantities (other than the dislocation angle) obtained from the large scale yielding model are greater than those calculated under the assumption of the small scale yielding. As expected, for very small values of the applied load the two models give relatively close results because in that range the dislocation length is small compared to the fracture length (Figs 2, 3). The calculated quantities increase abruptly as $t \to 1$ indicating large scale yielding. In this region we see significant deviation of the large scale yielding results (Fig.3) from the results of the small scale yielding (Fig.2) which were obtained under the assumption of $l \ll \alpha$.

Though the results of both figures show the same tendency we will focus next on the results of Fig.3 which are valid for any degree of yielding and are particularly important for short fractures as in those cases it is expected that the size of plastic zones could be comparable to the fracture length. For the problem at hand, it is important to consider short fractures as any fracture more likely will initiate from a pre-existing crack or a short fracture. The parameter of Eq. (15), which in general dictates the scale of plastic yielding for a von Mises material, can take values between 0 and 1. For value 0 the material is nearly elastic or brittle during fracturing. For increasing value of *t* the scale of plastic yielding increases. The limit value of this parameter is 1 which corresponds to material that will yield everywhere requiring infinite energy for mode-1 fracturing. If we assume that the stress field is isotropic (horizontal stresses are equal), for a fracture that propagates in the horizontal direction the parameter t will be close to 0 and the

fracture will propagate in a nearly brittle mode. On the other hand, if the fracture propagates vertically, as the vertical insitu stress is usually greater than the horizontal stresses, the value of t will be greater than 0 with a maximum value approaching 1. As the value of t is increasing towards 1 the size of the plastic zones becomes important relative to the fracture length (green line). In fact for values of t approaching 1 the energy dissipated in the plastic zones grows asymptotically (pink lines) to infinity which suggests that any energy provided for propagating the fracture will be dissipated in the plastic deformation and no mode-1 propagation will take place. The short fracture will inflate to a balloon kind of shape of a maximum width (light blue line) without propagating.

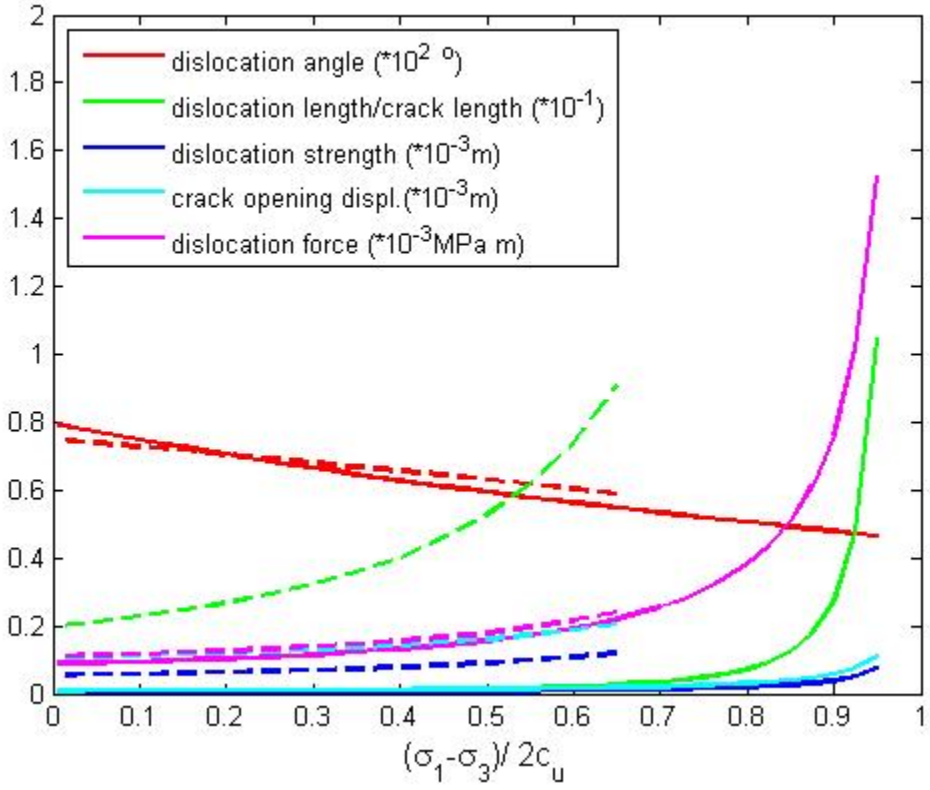

Fig.2. Calculated quantities vs ductility number for undrained analysis and small scale yielding with material original values (solid lines) and impaired values (dashed lines).

Figures 2 and 3 show also the results for the case that the rock properties impaired to extreme degree by the CO2 corrosive action (dashed lines). The results show that for the damaged material all the calculated quantities have increased significantly suggesting that larger plastic zones are developed (green lines) and much higher energy is dissipated (pink lines)

resulting to a more balloon type of fracture (light –blue lines). In fact, the limit for propagating a mode-1 fracture has moved to the left imposing a limit to the vertical insitu stress above which no hydraulic fracture will propagate vertically.

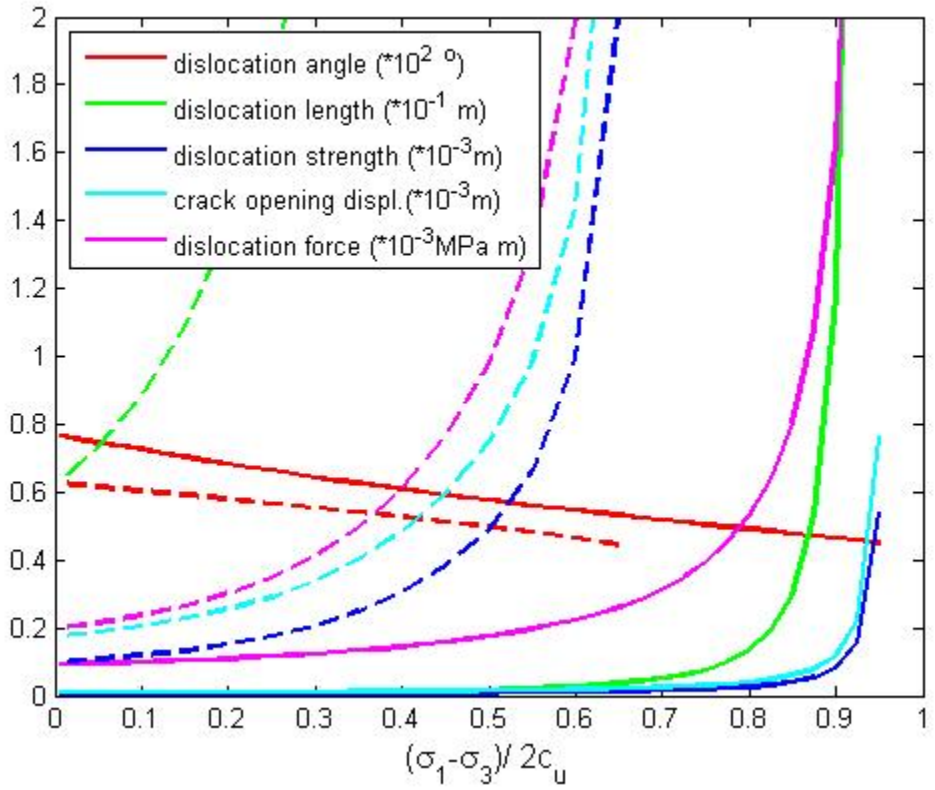

Fig.3. Calculated quantities vs ductility number for undrained analysis and large scale yielding with material original values (solid lines) and impaired values (dashed lines).

4.3 Frictional material

Figure 4 shows the results for a frictional material and drained conditions. This analysis will be valid in slow hydraulic fracturing operations in permeable materials such as sandstones. In this case the dominant parameter *t* takes the full expression of Eq.(14) varying, as before, between 0 and 1, with the value of 0 to correspond to brittle propagation and 1 to a fracture that requires infinite energy release per unit advance. The values between 0 and 1 correspond to fracture propagation of increasing ductility from brittle to small scale and finally to large scale yielding. As in the case of the undrained analysis, a horizontal fracture, which corresponds to t close to 0,

is more likely to propagate in a brittle mode compared to a vertical fracture which is more likely to propagate in a ductile mode for *t* approaching 1.

The dashed lines in Fig.4 show the results of the model with rock properties impaired by the CO2 corrosive action. For the damaged material the limit beyond no fracture will propagate in mode-1 has moved to the left. Close to that limit all the predicted quantities have greater values than in the case of the original material suggesting that the damaged material exhibits more ductile behavior compared to the original one.

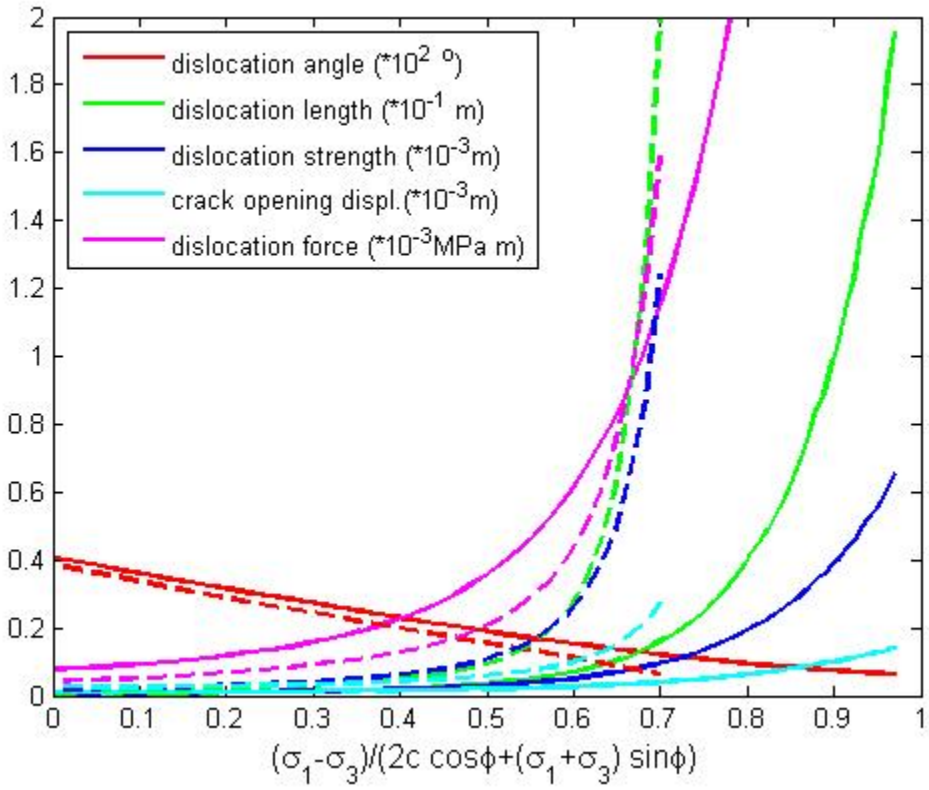

Fig.4. Calculated quantities vs ductility number for drained frictional analysis and large scale yielding with material original values (solid lines) and impaired values (dashed lines).

In Figures 3 and 4 the results at the RHS of the curves are interpreted to correspond to a fracture front that propagates vertically where as moving to the LHS the results correspond more to a fracture front that propagates horizontally. It is clear that much higher energy is dissipated in plastic deformation around the tip of the fracture that propagates vertically. For example in undrained conditions (Fig.3 and Table 3) for a vertical propagation in a stress field of σ_1/σ_3= 1.76 which corresponds to $t = 0.95$, we found that 117 times more energy is dissipated in plastic

deformation than the energy that is dissipated in a fracture that propagates horizontally in an isotropic stress field, which corresponds to $t = 0$. For this example, the profile of the fracture that its front propagates vertically will be 86 times wider than the profile of the fracture that its front propagates horizontally. For the damaged material the energy that is dissipated in a horizontal propagation is more than 2 times and the resulting fracture profile 20 times wider than for the case of the fracture embedded in the original material. For the damaged material a fracture will not propagate in a stress field with ratio above σ_1/σ_3= 1.05 which corresponds to $t = 0.650$. At this stress limit the dissipated energy for a vertical propagation will be 20 times higher and the resulting profile 16 times wider than in the case of a fracture front that propagates horizontally.

Similar results were found for the case of frictional analysis (Fig.4 and Table 3). For example, for a vertical propagation in a highly anisotropic stress field of σ_1/σ_3= 3.64 which corresponds to $t = 0.971$, we found that 100 times more energy is dissipated in plastic deformation than the energy that is dissipated in a fracture that propagates horizontally in an isotropic stress field which corresponds to $t = 0$. The profile of the fracture that its front propagates vertically will be 18 times wider than the profile of the fracture that its front propagates horizontally. For the damaged material the energy that is dissipated in a horizontal propagation is comparable but the resulting fracture profile is 3 times wider than for the case of the fracture embedded in the original material. For the damaged material, a fracture will not propagate in a stress field with ratio greater than σ_1/σ_3= 2.12 which corresponds $t = 0.7$. At this stress limit the dissipated energy for a vertical propagation will be 38 times higher and the resulting profile 12 times wider than in the case of a fracture front that propagates horizontally.

These findings support the argument that a hydraulically induced fracture from CO2 injection is more likely to propagate horizontally with high probability to remaincontained in the storage zone. The horizontal fracture propagation will have a positive effect on the injectivity and storage capacity of the formation. The containment in the vertical direction will mitigate the risk of fracturing and migration of CO2 in upper layers and back to the atmosphere. Though the corrosive effect of CO2 is expected to decrease the resistance to fracturing by decreasing the rock toughness, the overall decrease of rock strength from the CO2 corrosive action, e.g. through

a decrease of cohesion, promotes the ductile behavior with the provided energy to dissipate in plastic deformation and hence to mitigate the mode-1 fracture propagation.

Frictionless material or undrained analysis			
		Horizontal propagation	Vertical propagation
Virgin material	σ_1/σ_3 (t)	1 (0)	1.76 (0.950)
K_{IC}=1 MPa $m^{1/2}$	SER (MPa. m)	0.0000918	(X 117) 0.0107966
C_u=10 MPa	COD (m)	0.0000089	(X 86) 0.0007648
Damaged material	σ_1/σ_3 (t)	1.0 (t=0)	1.05 (t=0.650)
K_{IC}=0.1 MPa $m^{1/2}$	SER (MPa. m)	0.0001978	(X 20) 0.0040274
C_u=1 MPa	COD (m)	0.0001758	(X 16) 0.0028229
Frictional material or drained analysis			
Virgin material			
K_{IC}=1 MPa $m^{1/2}$	σ_1/σ_3 (t)	1.0 (t=0)	3.64 (t=0.971)
C=10 MPa	SER (MPa. m)	0.000077	(X 100) 0.007673
$\Phi=30^0$	COD (m)	0.000008	(X 18) 0.000141
Damaged material			
K_{IC}=0.1 MPa $m^{1/2}$	σ_1/σ_3 (t)	1.0 (t=0)	2.12 (t=0.7)
C=1 MPa	SER (MPa. m)	0.000042	(X 38) 0.001590
$\Phi=30^0$	COD (m)	0.000024	(X 12) 0.000272

Table 3. Strain Energy Release Rate (SER) and Crack Opening Displacement (COD) for frictionless and frictional material with virgin and degraded properties in horizontal and vertical fracture propagation

5 CONCLUSIONS

In this paper we presented a study on one of the potential mechanisms of CO2 migration from the geological storage site to upper formations and back to the atmosphere through induced mode-1 hydraulic fracturing of the formation. We built and extended an earlier work on the modeling of hydraulic fracturing in weak formations to study in particular the risk of hydraulic fracturing in the vertical direction vs hydraulic fracturing in the horizontal direction. Furthermore, as it is expected that CO2 injection in supercritical conditions due to its corrosive action will change the mechanical properties of the reservoir and cap rock we studied the same risk by modifying the mechanical parameters of the rock to extreme degree.

The study was based on an analytical Mohr-Coulomb dislocation fracturing model that was extended to account for fracture toughness and large scale plasticity that may develop around the hydraulic fracture tip. The analytical model enables the identification of a dominant parameter (14) which defines the regimes of brittle to ductile propagation and the limit at which a fracture requires infinite energy to propagate in mode-1. We found that a hydraulically induced fracture from CO2 injection is more likely to propagate horizontally than vertically, remaining contained in the injected storage zone. The horizontal fracture propagation will have positive effects on the injectivity and storage capacity of the formation. The containment in the vertical direction will mitigate the risk of fracturing and migration of CO2 to upper layers and back to the atmosphere. Though the corrosive effect of CO2 is expected to decrease the rock toughness and at first the resistance to fracturing, the overall decrease of the rock strength promotes the ductile behavior with the energy to dissipate in plastic deformation and hence to mitigate the mode-1 fracture propagation. We recognize that in the ductile regime and close to the limit at which a fracture requires high energy to propagate in mode-1, there is potential risk for initiation of shear fractures which may connect with other preexisting fractures and faults. The detailed investigation of this mechanism is not addressed in this paper and is currently part of a continuing research on the topic.

ACKNOWLEDGEMENT

This research was part of the project “DIDAKTOR/0311/58- The risk of formation fracturing from CO2 sequestration in geological formations” which was co-financed by the European

Regional Development Fund and the Cyprus Research Promotion Foundation and the project "GEOMECS THALES - Geomechanics and environment of CO2 geological storage'' which was co-financed by Greece and the European Union.

REFERENCES

1. International Energy Association, (2015) reports http://www.iea.org/topics/climatechange/

2. European Commission, Directive 2009/31/EC of the European Parliament and of the Council of 23 April 2009 on the geological storage of carbon dioxide and amending Council Directive 85/337/EEC, European Parliament and Council Directives 2000/60/EC, 2001/80/EC, 2004/35/EC, 2006/12/EC, 2008/1/EC and Regulation (EC) No. 1013/2006. Official Journal of the European Union 2009; 5(6): 114–145.

3. Metz B, Davidson O, de Coninck H, Loos M, Meyer L. *(eds). IPCC Special Report on Carbon Dioxide Capture and Storage. Cambridge University Press:* Cambridge, United Kingdom and New York, USA 2005.

4. Celia MA, Bachu S, Nordbotten JM, Gasda SE, Dahle HK. Quantitative estimation of CO2 leakage from geological storage: Analytical models, numerical models, and data needs. *In Greenhouse Gas Control Technologies 7,* Rubin ES, Keith DW, Gilboy CF, Wilson M, Morris T, Gale J, Thambimuthu K, *(eds.). Elsevier Science Ltd,* Oxford, 2005*;* 663–671.

5. Nordbotten, JM, Celia MA. Similarity solutions for fluid injection into confined aquifers. *Journal of Fluid Mechanics* 2006; **561**: 307-327.

6. Dentz M, Tartakovsky D. Abrupt-interface solution for carbon dioxide injection into porous media. *Transport in Porous Media* 2009; **79**: 15-27.

7. Sarris E, Gravanis E, Papanastasiou P. Investigation of self-similar interface evolution in carbon dioxide sequestration in saline aquifers. *Transport in Porous Media* 2014; **103**:341–359.

8. Bachu S, Bonijoly D, Bradshaw J, Burruss R, Holloway S, Christensen NP, Mathiassen OM. CO2 storage capacity estimation: methodology and gaps. *International Journal of Greenhouse Gas Control* 2007; **1:**430–443.

9. Vallin V, Pereira JM, Fabbri A, Wong H. Numerical modelling of the hydro-chemo-mechanical behaviour of geomaterials in the context of CO2 injection. *International Journal for Numerical and Analytical Methods in Geomechanics* 2013; **37**:3052–3069.

10. Bemer J, Lombard JM. From injectivity to integrity studies of CO2 geological storage. Chemical alteration effects on carbonates petrophysical and geomechanical properties. *Oil & Gas Science and Technology* 2010; **65**:445–459.

11. Wojtacki K, Lewandowska J, Gouze Ph, Lipkowski A. Numerical computations of rock dissolution and geomechanical effects for CO2 geological storage. *International Journal for Numerical and Analytical Methods in Geomechanics* 2015; **39**:, 482–506.

12. Samuelson J, Spiers C. J. Fault friction and slip stability not affected by Co2 storage: Evidence from short-term laboratory experiments on North Sea reservoir sandstones and caprocks. *International Journal of Greenhouse Gas Control* 2012; **11**:78–90. doi:10.1016/j.ijggc.2012.09.018

13. Papanastasiou P, Atkinson C. Representation of crack-tip plasticity in pressure sensitive geomaterials. *International Journal of Fracture* 2000; **102**: 271-286.

14. Papanastasiou P, Atkinson C. Representation of crack-tip plasticity in pressure-sensitive geomaterials: Large scale yielding. *International Journal of Fracture* 2006; **139**: 137-144.

15. Papanastasiou P,. Thiercelin M. Influence of inelastic rock behaviour in hydraulic fracturing. International Journal of Rock Mechanics and Mining Sciences 1993; **30**(7): 1241-1247.

16. Papanastasiou P. The influence of plasticity in hydraulic fracturing. *International Journal of Fracture* 1997; **84**: 61-79.

17. Papanastasiou P. The effective fracture toughness in hydraulic fracturing. *International Journal of Fracture* 1999; **96**: 127-147.

18. Sarris E, Papanastasiou P. Numerical Modelling of fluid-driven fractures in cohesive poro-elastoplastic continuum. *International Journal for Numerical and Analytical Methods in Geomechanics* 2013; **37** (12): 1822-1846.

19. van Dam DB, Papanastasiou P, de Pater CJ. Impact of rock plasticity on hydraulic fracture propagation and closure. *Journal of SPE Production & Facilities* 2002;**17** (3): 149-159.

20. Rice JR. A path-independent integral and the approximate analysis of strain concentration by notches and cracks. *Journal of Applied Mechanics Transaction ASME* 1968; **35**:379–386.

21. Tjioe M, Borja RI. On the pore-scale mechanisms leading to brittle and ductile deformation behavior of crystalline rocks. *International Journal for Numerical and Analytical Methods in Geomechanics* 2015. DOI: 10.1002/nag.2357.

22. Atkinson C, Kanninen MF. A simple representation of crack tip plasticity: The inclined strip-yield superdislocation model. *International Journal of Fracture* 1977; **13**: 151-163.

23. Papanastasiou P, Atkinson C. The brittleness index in hydraulic fracturing, ARMA 15-489; 7 pp, 2015

24. Holt RM, Fjær E, Nes OM, Alassi HT. A shaly look at brittleness. ARMA 11-366; 10 pp., 2011

25. Holt RM, Fjær E, Stenebraten JF, Nes OM. Brittleness of Shales: Relevance to borehole collapse and hydraulic fracturing. *Journal of Petroleum Sciences and Engineering* 04/2015; 131. DOI:10.1016/j.petrol.2015.04.006

26. Rohmer J, Allanic C, Bourgine B, Sulem ., Suhett-Helmer G, Ghabezloo S, Pouya A, Renard F, Beucher H, Mehl C, Siavelis M, Tardieu N. Improving our knowledge on the hydro-chemo-mechanical behaviour of fault zones in the context of CO2 geological storage. *Energy Procedia* 2014;**63**: 3371 – 3378.